ARTICLES

Journal of Semiconductors
(2020) 41, 012301
doi: 10.1088/1674-4926/41/1/012301

Quantum cascade superluminescent light emitters with high power and compact structure

Jialin Sun[1, 4], Chuncai Hou[2, 3, 4], Hongmei Chen[4], Jinchuan Zhang[2], Ning Zhuo[2], Jiqiang Ning[5], Changcheng Zheng[6], Zhanguo Wang[2], Fengqi Liu[2], and Ziyang Zhang[1, 4, †]

[1]School of Nano Technology and Nano Bionics, University of Science and Technology of China, Hefei 230026, China

[2]Key Laboratory of Semiconductor Materials Science, Institute of Semiconductors, Chinese Academy of Sciences, Beijing 100083, China

[3]The 718th Research Institute of China Shipbuilding Industry Corporation, Handan 056027, China

[4]Key Laboratory of Nanodevice and Applications, Suzhou Institute of Nano-Tech and Nano-Bionics, Chinese Academy of Sciences, Suzhou 215123, China

[5]Vacuum Interconnected Nanotech Workstation, Suzhou Institute of Nano-Tech and Nano-Bionics, Chinese Academy of Sciences, Suzhou 215123, China

[6]Division of Natural and Applied Sciences, Duke Kunshan University, Kunshan 215316, China

Abstract: Quantum cascade (QC) superluminescent light emitters (SLEs) have emerged as desirable broadband mid-infrared (MIR) light sources for growing number of applications in areas like medical imaging, gas sensing and national defense. However, it is challenging to obtain a practical high-power device due to the very low efficiency of spontaneous emission in the intersubband transitions in QC structures. Herein a design of ~5 μm SLEs is demonstrated with a two-phonon resonance-based QC active structure coupled with a compact combinatorial waveguide structure which comprises a short straight part adjacent to a tilted stripe and to a J-shaped waveguide. The as-fabricated SLEs achieve a high output power of 1.8 mW, exhibiting the potential to be integrated into array devices without taking up too much chip space. These results may facilitate the realization of SLE arrays to attain larger output power and pave the pathway towards the practical applications of broadband MIR light sources.

Key words: quantum cascade; superluminescent diode; mid-wave infrared

Citation: J L Sun, C C Hou, H M Chen, J C Zhang, N Zhuo, J Q Ning, C C Zheng, Z G Wang, F Q Liu, and Z Y Zhang, Quantum cascade superluminescent light emitters with high power and compact structure[J]. *J. Semicond.*, 2020, 41(1), 012301. http://doi.org/10.1088/1674-4926/41/1/012301

1. Introduction

Quantum cascade (QC) superluminescent light emitters (SLEs), different from traditional bipolar semiconductor emitters, are unipolar semiconductor broadband edge-emitting light sources based on intersubband transition of electrons in the conduction band[1, 2]. QC SLEs are playing increasingly significant roles in mid-infrared (MIR) applications, such as medical imaging, gas sensing, and national defense[3–5]. As an important example of medical imaging, QC SLEs could be used as the light sources in MIR optical coherence tomography (OCT) systems[6, 7]. OCTs in visible and near-infrared (NIR) ranges have been developed as an effective technique for non-contact and non-invasive imaging of inhomogeneous human tissue samples[8–10]. However, most biological tissues absorb less photons in visible or NIR spectrum compared to that in the MIR region[11–13]. Therefore, a MIR-OCT system could become a much more promising technique for medical imaging of biological tissues because of its higher resolution.

SLEs based on QC material are the ideal broadband light sources for the MIR-OCT systems[14]. However, it is very challenging to achieve sufficient high output power for the QC SLEs due to the very low efficiency of spontaneous emission caused by the very short nonradiative carrier lifetime in QC structures[1]. Previously, in the interest of suppressing lasing by adopting an extremely low reflectivity to obtain sufficient superluminescence, bulky or complex waveguide structures are usually designed using methods like anti-reflection (AR) coating, large inclined angle of 17° or spiral cavity with large bend radius in the devices[15–17]. But these device structures always sacrifice the light emission from one cleaved facet, leading to substantial optical loss and low conversion efficiency. As a result, the previous reported QC SLEs were only able to operate at low temperature and with low duty cycle of about 0.05%[16]. Besides continuing to further improve the output power from a single device, fabricating emitter arrays is another effective way for this purpose[18]. However, previously reported device structures mentioned above experienced serious heat problem which limited the on-chip miniaturization and encapsulation. Meanwhile, their large inclined angle and device geometry made themselves not suitable for the fabrication of compact light emitter arrays.

In this paper, a strain-compensated QC material based on a four-quantum well (QW) coupling and two-phonon resonance structure was utilized to improve the efficiency of amplified spontaneous emission in the intersubband transitions.

Correspondence to: Z Y Zhang, zyzhang2014@sinano.ac.cn
Received 19 SEPTEMBER 2019; Revised 14 OCTOBER 2019.

Based on this QC active region, a combinatorial waveguide structure was demonstrated with a short straight waveguide (SW) adjacent to a tilted waveguide (TW) and to a J-shaped waveguide (JW). This structure would produce two structural mutations to realize a rather low reflectivity with a fairly small geometry and enable the fabrication of long device on a relatively small chip area. Benefiting from these material and device structural designs, the fabricated SLEs have inhibited lasing and achieved a high superluminescent power of 1.8 mW at 80 K in quasi-continuous wave (quasi-CW) mode with a duty circle of 3%. Furthermore, these attempts would facilitate the integration of SLE arrays to attain larger output power and practical applications as broadband MIR light sources in the next step.

2. Experiments

The active region of QC SLEs was grown by solid source molecular beam epitaxy (MBE) in a single growth step on an InP substrate, which consists of the strain-compensated four-QW coupling of $In_{0.678}Ga_{0.322}As/In_{0.365}Al_{0.635}As$ and two-phonon resonance structure. The two-phonon resonance leads to a more efficient electron extraction due to the twice electron pumping by optical phonon scattering. As a result, this structure substantially benefits the population inversion and then enhances the radiative transition rate. Thirty repetitions of the active region/injector are sandwiched by low doped ($n \approx 8 \times 10^{16}$ cm^{-3}) $In_{0.53}Ga_{0.47}As$ layers. Beginning from the injection barrier, the layer sequence of one period is as follows (thickness in nanometers): **3.8**/1.2/**1.3**/4.3/**1.3**/3.8/**1.4**/3.6/**2.2**/2.8/**1.7**/2.5/**1.8**/2.2/**1.9**/2.1/**2.1**/2.0/**2.1**/1.8/**2.7**/1.8. The $In_{0.678}Ga_{0.322}As$ quantum well layers are shown in regular numbers, the $In_{0.365}Al_{0.635}As$ barrier layers are shown in bold numbers, and the doped layers (Si, 1.5×10^{17} cm^{-3}) are underlined. Fig. 1(a) illustrates the band structure of the four-QW coupling and two-phonon resonance-based QC structure for ~5 μm wavelength emission, and Fig. 1(b) shows the corresponding layered cross-sectional structure of the QC material.

After the MBE growth, the wafer was processed into a 10 μm double-trench narrow ridge waveguide structure by photolithography and wet chemical etching. The waveguide was etched deeply down to 7 μm through the active region to avoid the pronounced current spreading caused by the strong discontinuities of the anisotropic electrical conductivity in the multi-quantum well active region. Fig. 2(a) exhibits the schematic diagram of the double-trench narrow ridge waveguide structure, which is capable of creating a sufficient low reflectivity by the three-section design: a 0.5-mm-long SW adjacent to a 1-mm-long TW and to a 12°-bent 2-mm-long JW. Fig. 2(b) shows the corresponding scanning electron microscope image of the straight end, and Figs. 2(c) and 2(d) present the top-view microscope images of SLE devices with 8°- or 12°-inclined TW, respectively. These images have indicated the high quality of the device fabrication without any observable defect or irregularity. Then, an insulation layer of SiO_2 was deposited using plasma-enhanced chemical vapor deposition. The 3-μm-wide contact windows were fabricated on top of the ridges by the techniques of photolithography and reactive ion etching, and the Ti/Au (50/500 nm in thickness) top metal contact was deposited by magnetron sputtering. Afterwards, the wafer was thinned and burnished to

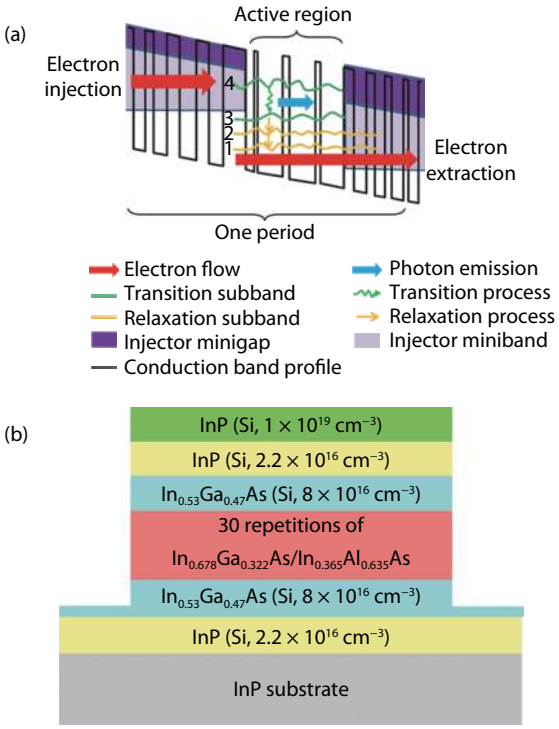

Fig. 1. (Color online) Illustration of (a) the band structure of the four-QW coupling and two-phonon resonance-based QC structure, and (b) the corresponding layered cross-sectional structure of the QC material.

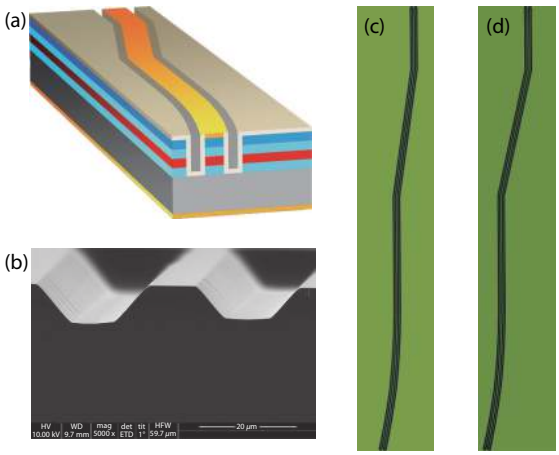

Fig. 2. (Color online) (a) Schematic diagram of the double-trench narrow ridge waveguide structure of SLE devices. (b) Corresponding scanning electron microscope image of the straight end. The top-view microscope images of SLE devices with (c) 8°- or (d) 12°-inclined TW.

about 110 μm, and the Ge/Au/Ni/Au (30/50/15/200 nm in thickness) bottom metal contact was evaporated on the burnished reverse side by electron beam evaporation. Finally, the samples were mounted epitaxial-side down on copper heat sinks to relieve the self-heating effect.

3. Results and discussion

The superluminescent light is generated from spontaneous emission and amplified by stimulated emission below the lasing threshold, which is similar to the design of lasers but with the suppression of light oscillations in resonators. It is well known that a tilted or bent waveguide design with relatively small angles cannot offer low reflectivity of $< 10^{-6}$

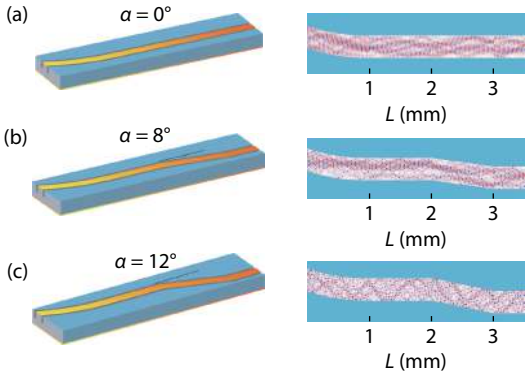

Fig. 3. (Color online) Schematic drawings (left) and optical field simulations (right) of the SLEs with (a) $\alpha = 0°$, (b) $\alpha = 8°$, or (c) $\alpha = 12°$, respectively.

to inhibit lasing in the MIR QC SLEs[19]. As a result, a 17°-inclined waveguide was used in the previous report to achieve such a low reflectivity, but this design limited the on-chip miniaturization and encapsulation[16, 17, 19, 20]. Moreover, from our previous work[19, 20], a mutation of refractive index in the waveguide structure of a QC SLE is the key point to realize high-quality superluminescent emission. A novel device structural design which combines various waveguide geometries, may produce reflectivity mutation and make possible the device miniaturization. In this work, a sectionalized device structure was demonstrated to create two jumps of refractive index in the waveguide to achieve a sufficient low reflectivity within a fairly small geometry, and hence support the integration of SLE arrays.

As the inclined angle of TW is the critical factor to acquire such a reflectivity, optical field simulations were performed to find an appropriate inclined angle (denoted as α). The schematic drawings of different waveguide structures with $\alpha = 0°$, 8° or 12° (on the left) and the corresponding simulated mode distribution results (on the right) are shown in Figs. 3(a)–3(c), respectively. The waveguide with $\alpha = 0°$ is equivalent of a single JW with bent angle of 12°, which is obviously not able to suppress lasing[19]. The corresponding mode distribution shown in Fig. 3(a) exhibits that there is only one main body of mode in the waveguide leading to the lasing emission. A similar mode distribution remains in the waveguide when α rises to 6°, 8° or 10°, shown in Fig. 3(b) (taking $\alpha = 8°$ as a representative), indicating that the guided light would most probably continue to generate lasing despite the emergence of more and more optical modes. The lasing could be inhibited as various optical modes appear in the waveguide when $\alpha = 12°$, shown in Fig. 3(c), which might provide a suitable low reflectivity to realize strong superluminescent emission. When α further rises to 14°, the mode distribution changes little, but the waveguide with a lower reflectivity, which leads to more optical loss. In order to check our simulations and acquire the desirable SLEs, a series of devices were designed and fabricated.

The emission characteristics of the fabricated SLEs were measured from the bent end (front facet, the left end in Fig. 3), which has smaller reflectivity than the straight end (rear facet). The light–current (L–I) curves were collected by a calibrated thermopile detector placed directly in front of the cryostat, and the emission spectra were measured by a Fourier transform infrared spectrometer. As seen in Fig. 4(a),

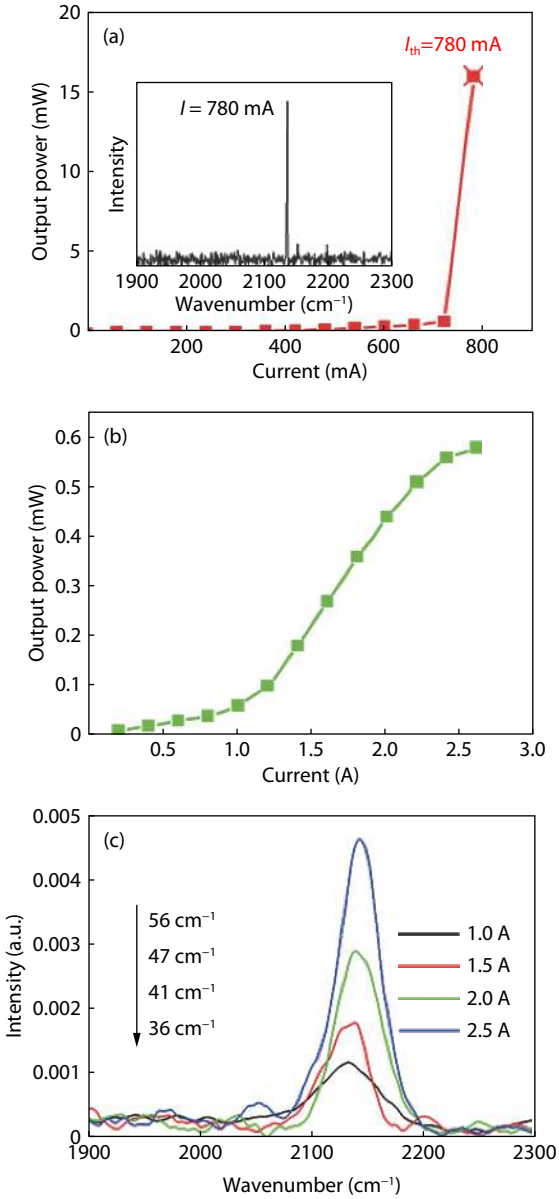

Fig. 4. (Color online) Emission characteristics of SLEs measured under quasi-CW (15 kHz, 2 μs) mode at 80 K: (a) L–I curve of the SLE with $\alpha = 8°$, and the inset is the corresponding lasing spectrum at 780 mA; (b) L–I curve and (c) emission spectra of the coated SLE.

the SLEs with $\alpha = 8°$ exhibit lasing characteristics rather than superluminescence at 80 K in quasi-CW (15 kHz, 2 μs) regime, and the pulsed threshold current is found to be about 780 mA. In Fig. 4(a), the "×" marks the lasing threshold, which is determined from the corresponding spectrum shown in the inset. This experimental observation illustrates that the waveguide structure of such an SLE with $\alpha = 8°$ could not provide a sufficient low reflectivity to suppress lasing and generate superluminescent light, which conforms to the simulation results.

Then, the SLEs with $\alpha = 8°$ were improved by introducing an Al_2O_3/Ge (450/35 nm in thickness) AR coating on the rear facet to further suppress lasing. The L–I curve and emission spectra of such an SLE are shown in Figs. 4(b) and 4(c), which were measured at 80 K in the quasi-CW (15 kHz, 2 μs) mode. Lasing was completely suppressed by the AR coating, and superluminescent light emission was observed from the front facet. The output power increases super linearly as

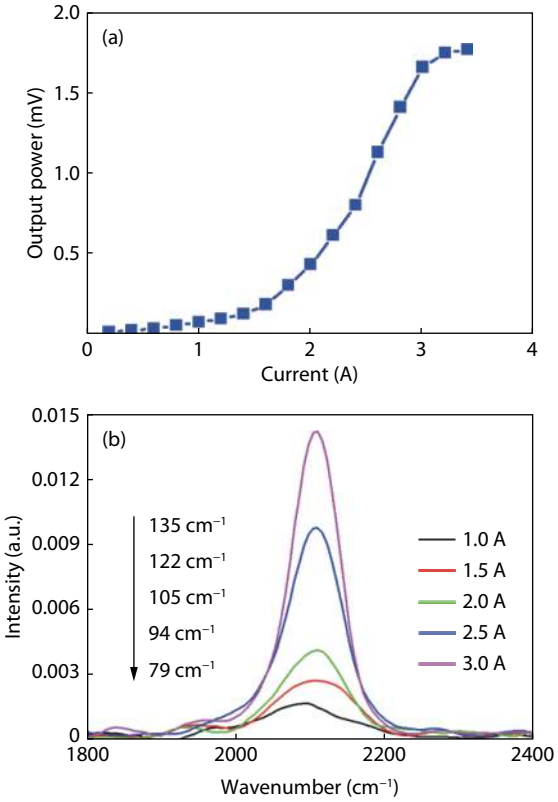

Fig. 5. (Color online) (a) *L–I* curve and (b) emission spectra of SLEs with $\alpha = 12°$ measured under quasi-CW (15 kHz, 2 μs) regime at 80 K.

a function of injected current, and the maximum superluminescent power is 0.6 mW at 2.6 A. The spectral curves exhibit smooth Gaussian shape, and the full width at half maximum (FWHM) is 36 cm^{-1} when the optical gain has saturated. The fairly narrowband superluminescent output of the coated SLE indicates that the AR coating can only reluctantly inhibit lasing in this structure. Meanwhile, the output power is also relatively low due to the substantial optical loss caused by the AR coating. Therefore, the waveguide structure with $\alpha = 8°$ is not suitable for fabricating high-power and broadband MIR SLEs.

To obtain more desirable MIR SLEs, the SLEs with $\alpha = 12°$ were fabricated according to the simulation results. Fig. 5 exhibits the emission characteristics of such a SLE at 80 K in quasi-CW (15 kHz, 2 μs) mode. As seen from the *L–I* curve in Fig. 5(a), a high output power of 1.8 mW, which is three times than that of the coated SLEs with $\alpha = 8°$, has been obtained at the current of 3.2 A. The Gaussian shaped spectra at different currents are shown in Fig. 5(b), and the FWHM decreases from 135 to 79 cm^{-1} with increasing current, which is much wider than that of coated SLEs with $\alpha = 8°$. A broad spectral width means a short coherence length, which plays an important role in the imaging quality of OCT systems. The coherence length decides the depth resolution of 3D images, so a short coherence length is appealing for high quality imaging[21]. Furthermore, the SLEs with $\alpha = 12°$ are able to operate at room temperature (RT), but the corresponding output power is much less.

It is well known that integrating several single emitters into a compact array is an effective approach to obtain high output power. However, the structure of array devices is certainly more complicated compared with single ones, so more difficulties need to be overcome to design and fabricate SLE arrays. We believe that the fairly small waveguide geometry and uniform structural width of this type of SLEs are quite favourable candidates for the array fabrication.

4. Conclusion

In conclusion, a monolithic integrated waveguide structure was designed according to theoretical analysis and optical field simulation, containing three sections: a short straight part, a tilted stripe and a JW structure. Based on this waveguide design and a strain compensated QC active material, a type of compact MIR SLEs was fabricated, which has achieved a high output power of 1.8 mW with a corresponding spectral width of 79 cm^{-1} at 80 K in quasi-CW (15 kHz, 2 μs) regime. This work suggests the possibility to build integrated compact array devices based on this promising structural design to reach sufficient high-power and stable RT operation, and might promote the actual applications of broadband MIR light sources, such as in MIR-OCT systems.

Acknowledgments

This work was supported by the Key Research and Development Plan of Ministry of Science and Technology (No. 2016YFB0402303), the National Natural Science Foundation of China (No. 61575222), the open project of the State Key Laboratory of Luminescence and Applications, and China Postdoctoral Science Foundation (No. 2017M621858).

References

[1] Faist J, Capasso F, Sivco D L, et al. Quantum cascade laser. Science, 1994, 264(5158), 553
[2] Vitiello M S, Scalari G, Williams B, et al. Quantum cascade lasers: 20 years of challenges. Opt Express, 2015, 23(4), 5167
[3] Zhang Z Y, Hogg R A, Lv X Q, et al. Self-assembled quantum-dot superluminescent light-emitting diodes. Adv Opt Photonics, 2010, 2(2), 201
[4] Riedi S, Cappelli F, Blaser S, et al. Broadband superluminescence, 5.9 μm to 7.2 μm, of a quantum cascade gain device. Opt Express, 2015, 23(6), 7184
[5] Zia N, Viheriala J, Koivusalo E, et al. GaSb superluminescent diodes with broadband emission at 2.55 μm. Appl Phys Lett, 2018, 112(5), 051106
[6] Brezinski M E, Fujimoto J G. Optical coherence tomography: high-resolutionimaging in nontransparent tissue. IEEE J Sel Top Quantum Electron, 1999, 5(4), 1185
[7] Fujimoto J G, Pitris C, Boppart S A, et al. Optical coherence tomography: an emerging technology for biomedical imaging and optical biopsy. Neoplasia, 2000, 2(1/2), 9
[8] Zhang Z Y, Wang Z G, Xu B, et al. High-performance quantum-dot superluminescent diodes. IEEE Photon Technol Lett, 2004, 16(1), 27
[9] Jiang Q, Zhang Z Y, Hopkinson M, et al. High performance intermixed p-doped quantum dot superluminescent diodes at 1.2 μm. Electron Lett, 2010, 46(4), 295
[10] Chen S M, Zhou K J, Zhang Z Y, et al. Hybrid quantum well/quantum dot structure for broad spectral bandwidth emitters. IEEE J Sel Top Quant, 2013, 19(4), 1900209
[11] Seddon A B. Mid-infrared (IR) – a hot topic: the potential for using mid-IR light for non-invasive early detection of skin cancer in vivo. Phys Status Solidi B, 2013, 250(5), 1020
[12] Lopez-Lorente A I, Mizaikoff B. Mid-infrared spectroscopy for protein analysis: potential and challenges. Anal Bioanal Chem, 2016, 408(11), 2875

[13] Wang F F, Jin P, Wu J, et al. Active multi-mode-interferometer broadband superluminescent diodes. J Semicond, 2016, 37(1), 014006

[14] Zorin I, Su R, Prylepa A, et al. Mid-infrared Fourier-domain optical coherence tomography with a pyroelectric linear array. Opt Express, 2018, 26(25), 33428

[15] Zibik E A, Ng W H, Revin D G, et al. Broadband 6 μm < λ < 8 μm superluminescent quantum cascade light-emitting diodes. Appl Phys Lett, 2006, 88(12), 121109

[16] Aung N L, Yu Z, Yu Y, et al. High peak power ($\geqslant$ 10 mW) quantum cascade superluminescent emitter. Appl Phys Lett, 2014, 105(22), 221111

[17] Zheng M C, Aung N L, Basak A, et al. High power spiral cavity quantum cascade superluminescent emitter. Opt Express, 2015, 23(3), 2713

[18] Causa F, Burrow L. Ripple-free high-power super-luminescent diode arrays. IEEE J Quantum Electron, 2007, 43(11), 1055

[19] Hou C C, Chen H M, Zhang J C, et al. Near-infrared and mid-infrared semiconductor broadband light emitters. Light Sci Appl, 2018, 7, 17170

[20] Hou C C, Sun J L, Ning J Q, et al. Room-temperature quantum cascade superluminescent light emitters with wide bandwidth and high temperature stability. Opt Express, 2018, 26(11), 13730

[21] Fercher A F, Drexler W, Hitzenberger C K, et al. Optical coherence tomography —principles andapplications. Rep Prog Phys, 2003, 66, 239